This is a preproof accepted article for *Mineralogical Magazine*
This version may be subject to change during the production process
DOI: 10.1180/mgm.2025.10180

As-rich florencite-(La) inclusions in euclase and quartz from hydrothermal veins in Abaíra, Bahia, Brazil: evidence from EPMA, single-crystal X-ray diffraction and Raman spectroscopy

Luiza Almeida Villar de Queiroz[1], Ciro Alexandre Ávila[2], Filipe Barra de Almeida [3], Felipe Emerson André Alves[4], Mario Luiz de Sá Carneiro Chaves[1], Luiz Carlos Bertolino[1,4] and Jurgen Schnellrath[4]

[1] Programa de Pós-Graduação em Geociências da Universidade do Estado do Rio de Janeiro (PPGG - UERJ). Rua São Francisco Xavier, 524 - Maracanã, Rio de Janeiro - RJ, Brazil.

[2] Museu Nacional –UFRJ. Quinta da Boa Vista - São Cristóvão, Rio de Janeiro, RJ, Brazil.

[3] Universidade Federal Fluminense (UFF). Niteroi, RJ, Brazil

[4] Centro de Tecnologia Mineral (CETEM). Avenida Pedro Calmon, Ilha da Cidade Universitária, 21.941-908, Rio de Janeiro, RJ, Brazil.

Abstract

As-rich florencite-(La) occurs as microscopic inclusions within pink–orange euclase and quartz from auriferous hydrothermal veins in Abaíra, Bahia State, Brazil. Electron probe microanalysis indicates a predominance of phosphate over arsenate at the tetrahedral site. Single-crystal X-ray diffraction reveals slight unit-cell expansion in the As-rich variety. Raman spectroscopy detects both phosphate- and arsenate-related vibrational modes, along with weak OH-stretching and diffuse bands attributable to hydrogen-bonded species, indicating mainly structural hydroxyl with possible contributions from weakly bound H_2O. The mineral likely formed during a late hydrothermal stage involving progressive REE enrichment and oxidising, acidic fluid conditions. These findings emphasise the structural sensitivity of florencite-(La) to tetrahedral-site substitutions and hydrogen bonding, and its potential as a sensitive tracer of REE-enriched hydrothermal systems.

*luizavq@gmail.com

Keywords: As-rich florencite-(La), solid solution, REE, EPMA, single-crystal XRD, μ Raman spectroscopy.

Introduction

Rare-earth elements (REE) rank among the strategic raw materials for modern high-technology industries. These elements are typically concentrated in phosphate minerals such as monazite, but also occur in carbonates like bastnäsite and, less commonly, in members of the alunite supergroup, notably the florencite group. Within this group, classification into the plumbogummite and dussertite subgroups depends on whether phosphate (PO_4^{3-}) or arsenate (AsO_4^{3-}) anions dominate the tetrahedral site (Bayliss et al., 2010; Back, 2018).

The substitution of P^{5+} by As^{5+} in florencite-group minerals has been widely reported, but systematic crystal-chemical investigations of the florencite-(La)–arsenoflorencite-(La) solid solution remain limited. Reports of substitutions involving alternative tetrahedral groups are even rarer, particularly those concerning sulphate (SO_4^{2-}) in REE-bearing phases. In this context, it is important to note that if As were to predominate over P in the tetrahedral site, the correct mineralogical name would be arsenoflorencite-(La). Florencite-(La) was approved as a mineral species by the IMA in 1987 (IMA1987-s.p.; Lefebvre & Gasparrini, 1980), whereas arsenoflorencite-(La) was only recognised in 2009 (IMA2009-078; Mills et al., 2010). Historically, cerium-dominant analogues of this group have been more frequently described (Hussak & Prior, 1900; Nickel & Temperley, 1987).

This study describes the occurrence and crystal-chemical characterization of As-rich florencite-(La) as microscopic inclusions within pink-orange euclase (Fig. 1) and colourless quartz crystals from auriferous hydrothermal quartz veins in the Abaíra region, Bahia State, Brazil. The compositional variability along the PO_4^{3-}–AsO_4^{3-} solid solution was investigated

https://doi.org/10.1180/mgm.2025.10180 Published online by Cambridge University Press

using electron-probe microanalysis (EPMA) and single-crystal X-ray diffraction. Raman spectroscopy was further employed to evaluate the presence of hydroxyl groups, thereby providing additional constraints on the structure of this hydrated phase.

Figure 1. Rough pink-orange euclase crystal from Abaíra, Bahia, Brazil. Maximum crystal width: 22 mm.

Geological setting

The studied As-rich florencite-(La) crystals were recovered from hydrothermal veins located in the municipality of Abaíra, in the central region of Bahia State, Brazil (Chaves et al. 2025). These veins are hosted in quartzites of the Ouricuri do Ouro Formation, at the base of the Paraguaçu Group, and are in contact with metarhyolites from the upper portion of the Rio dos Remédios Group (Gilles-Guéry et al., 2022).

This geological domain belongs to the Espinhaço Supergroup, a Mesoproterozoic megasequence comprising thick packages of continental, marine, and volcanic/metavolcanic metasedimentary rocks deposited ca. 1.75–1.80 Ga (Guimarães et al., 2005). The Espinhaço units were deposited over Archean to Paleoproterozoic basement rocks of the São Francisco Craton and are stratigraphically divided into three main groups: (1) Serra da Gameleira; (2) Rio dos Remédios Group (Novo Horizonte and Lagoa de Dentro formations); and (3) Paraguaçu Group (Ouricuri do Ouro, Mangabeira, and Açuruá formations). Overlying these

https://doi.org/10.1180/mgm.2025.10180 Published online by Cambridge University Press

are the Chapada Diamantina Group (Tombador and Caboclo formations) and the younger Morro do Chapéu Formation (Guimarães et al., 2012).

Following deposition, the region underwent significant deformation during the Neoproterozoic Brasiliano Orogeny (~600–500 Ma), associated with the final amalgamation of Gondwana. This tectonic event resulted in crustal shortening, thickening, and the formation of major shear zones and fold-thrust belts, such as the Araçuaí Belt to the south (Almeida, 1967, 1977; Trompette, 1994). In the Chapada Diamantina region, deformation intensity increases from north to south but generally remains within the greenschist metamorphic facies (Torquato & Fogaça, 1981; Süssenberger et al., 2014). The genesis of most mineral deposits in the area, including gold, barite, rutilated quartz, and pyrophyllite, is associated with the circulation of low-temperature hydrothermal fluids during this orogenic episode (Guimarães et al., 2005; Teixeira et al., 2019).

U-Pb dating of xenotime-(Y) from quartz veins in the Rio dos Remédios Group yielded ages of 491.7 ± 1.0 Ma, 493.0 ± 0.93 Ma, and 504.1 ± 0.78 Ma (Chaves et al., 2018), confirming that the hydrothermal mineralization is temporally related to the late stages of the Brasiliano Orogeny.

https://doi.org/10.1180/mgm.2025.10180 Published online by Cambridge University Press

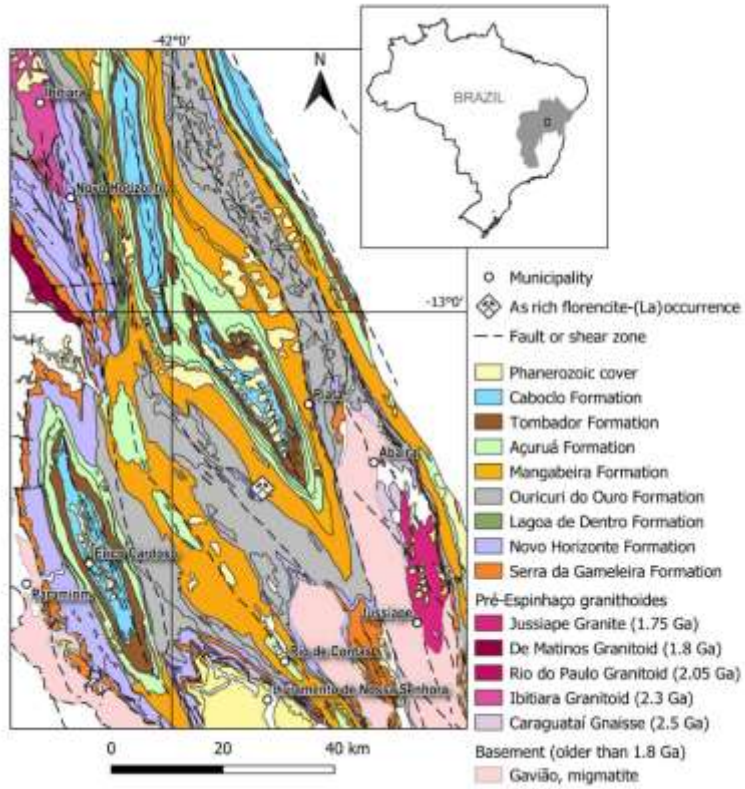

Figure 2. Map of Brazil at upper right showing the location of the São Francisco Craton. The highlighted rectangle indicates the area enlarged to display the geological sketch of the occurrence site of As-rich florencite-(La), modified from Guimarães et al. (2005).

Materials and methods

Microscopy and Imaging

Rough crystals of euclase ($BeAlSiO_4(OH)$) and quartz were examined under a Carl Zeiss Stemi 2000-C stereomicroscope using 1-bromonaphthalene as immersion medium to enhance contrast and identify inclusions. Photomicrographs were acquired using a Canon EOS 6D digital camera under transmitted polarized light.

Electron Probe Microanalysis (EPMA)

Quantitative chemical analyses were carried out using a CAMECA SXFive electron microprobe at the Electron Microprobe Laboratory, Institute of Geosciences, Federal University of Rio Grande do Sul (UFRGS). The instrument was equipped with five wavelength-dispersive spectrometers (WDS), an energy-dispersive spectrometer (EDS), and

https://doi.org/10.1180/mgm.2025.10180 Published online by Cambridge University Press

an optical microscope. Analyses were performed with an accelerating voltage of 15 kV, beam current of 20 nA, and a beam diameter of 1 μm. Counting times were 10 seconds at the peak, 5 seconds background for Al, P, As and La; 20 seconds at the peak and 10 seconds at the background for Ca, Ba and Nd; and 30 seconds at the peak and 15 seconds in the background for S, Ce, Pr, Sm, Dy and Si. Crystals used were TAP (Si, Al and As), LPET (Ca, P, S, Sr and Ba) and LLIF (Fe, REEs). To avoid peak overlaps, Lβ lines were used for Pr, Nd, Sm, and Dy.

Cation proportions were calculated using the normalization scheme of Janeczek and Ewing (1996), assuming six cations and 14 oxygen atoms per formula unit. Minor elements (S, Si) and As were considered as partial substitutes for P. Hydrogen content was estimated based on charge balance, assuming six hydroxyl groups per unit cell. The site occupancy model followed the general formula $DG_3(TX_4)_2X'_6$ as proposed by Smith et al. (1998) and Bayliss et al. (2010), with D, G, and T sites corresponding to 1, 3, and 2 cationic positions, respectively.

Single-Crystal X-ray Diffraction (SC-XRD)

Crystallographic analyses were conducted at the Multiuser X-ray Diffraction Laboratory (LDRX) of Universidade Federal Fluminense (UFF) using a Bruker D8 Venture diffractometer equipped with a graphite-monochromated MoKα source (λ = 0.71073 Å) and CMOS detector. Two crystals were analysed, one from a euclase inclusion and the other from a quartz inclusion. Data were collected at 273 K, with 2θ ranging up to 30.46° (sample 1) and 26.34° (sample 2), and a detector distance of 40 mm. Data reduction was performed using **SAINT**, and absorption corrections were applied via **SADABS**. Structural refinement was performed using **SHELX-18** within the **WinGX** suite, in space group $R\bar{3}m$, using initial atomic coordinates from the alunite structure model (Mills et al., 2010). The P/As site was

https://doi.org/10.1180/mgm.2025.10180 Published online by Cambridge University Press

refined with mixed occupancy and a vacancy of 0.03. All non-hydrogen atoms were refined anisotropically. Powder XRD was not conducted due to limited sample availability.

Raman Spectroscopy

Micro-Raman analyses were performed using a WITec alpha300 R Raman microscope at the Centro de Tecnologia em Nanomateriais e Grafeno (CTNano), Universidade Federal de Minas Gerais (UFMG). Spectra were acquired with a 532 nm laser (20 mW max power), 50× objective, and six accumulations of 5 s integration each, yielding ~5 cm^{-1} resolution. The spectra were collected in the 100–3800 cm^{-1} range at room temperature in random crystal orientations. Baseline correction was performed using **GRAMS**, and peak deconvolution was carried out with **PeakFit v.4.12**, applying Lorentzian-Gaussian mixed functions with minimal component fitting.

Results

General Description and Optical Microscopy Identification

Colourless to pale yellow, transparent minerals were observed as inclusions within euclase (Figure 3A) and quartz crystals (Figure 3B), measuring approximate 150 x 70 μm and 60 x 20 μm respectively. Under polarized transmitted light microscopy, the studied euhedral crystals exhibited rhombohedral and scalenohedral crystal forms, with a pseudo-cubic habit. These inclusions were commonly associated with other mineral phases such as dolomite, quartz, phyllosilicates, and cryptomelane–hollandite-type fibres and cylinders. Numerous negative crystals of varied and peculiar morphologies, as well as fluid inclusions, were also identified.

https://doi.org/10.1180/mgm.2025.10180 Published online by Cambridge University Press

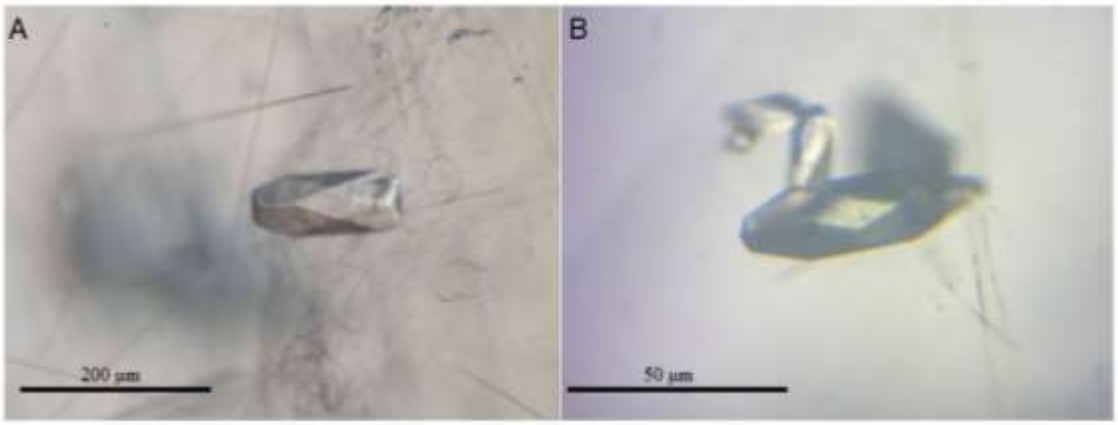

Figure 3. Euhedral crystals of As-rich florencite-(La) occurring as inclusions in; (a) pink-orange euclase, associated with woolly type inclusions; and (b) quartz crystals hosting fibrous inclusions.

Electron probe microanalyses

Nine spot analyses were obtained from different zones of a florencite-(La) inclusion occurring within the analysed euclase crystal. The EPMA data were recalculated on an anhydrous basis to derive cation proportions per formula unit (a.p.f.u.) for florencite-(La), based on 14 oxygen atoms. The general formula of the florencite–arsenoflorencite-(La) solid solution is expressed as $LaAl_3(PO_4,AsO_4)_2(OH)_6$, derived from the alunite supergroup formula $DG_3(TX_4)_2X'_6$, as proposed by Smith et al. (1998) and Bayliss et al. (2010).

In this structural model, the D site is typically occupied by large cations (REE^{3+}, Ca^{2+}, Sr^{2+}, Ba^{2+}, Pb^{2+}, etc.); the G site corresponds to a trivalent octahedral position, often occupied by Al^{3+} or Fe^{3+}, and occasionally by divalent or trivalent transition metals (Cu^{2+}, Zn^{2+}, V^{3+}); and the T site is tetrahedral, generally occupied by PO_4^{3-}, AsO_4^{3-}, SO_4^{2-}, or minor SiO_4^{4-}. The X/X′ sites are dominated by O^{2-} and OH^-, with minor incorporation of F^- and H_2O. Due to extensive potential for ionic substitution, these compositions often involve OH-for-O replacement in the tetrahedron, H_2O-for-OH substitution, and partial occupancy of cationic sites (Jambor, 1999; Dill, 2001).

https://doi.org/10.1180/mgm.2025.10180 Published online by Cambridge University Press

Table 1. Electron probe microanalysis (EPMA) data (n = 9) for As-rich florencite-(La) occurring as inclusions in euclase sample.

Oxide	Average (wt%)	Min	Max	Std.Dev.	Probe Std.
SiO_2	0.18	0.06	0.32	0.09	**$CaSiO_3$**
SO_3	0.31	0.08	0.50	0.16	**$SrSO_4$**
P_2O_5	15.80	12.47	18.61	2.07	**Apatite**
As_2O_5	15.61	12.22	19.61	2.86	**GaAs**
Al_2O_3	28.51	27.58	30.59	1.07	**Spodumene**
La_2O_3	24.44	23.08	25.73	0.88	**$LaPO_4$**
Ce_2O_3	0.22	0.13	0.30	0,05	**$CePO_4$**
Pr_2O_3	1.35	1.05	1.65	0,22	**$PrPO_4$**
Nd_2O_3	2.48	1.98	2.81	0.27	**$NdPO_4$**
Sm_2O_3	0.02	0	0.15	0.05	**$SmPO_4$**
Dy_2O_3	n.d.				**$DyPO_4$**
CaO	0.26	0.18	0.37	0.07	**$CaSiO_3$**
SrO	0.16	0.00	0.37	0.14	**$SrSO_4$**
BaO	n.d.	0	0	0	**$BaSO_4$**
$H_2O^*_{calc}$	9.90	9.80	10.04	0.10	
Total	99.22	98.59	100.02	0.60	
$\sum REE_2O_3$	28.51	26.24	30.64	1.47	

Tabela 2. Chemical composition of the As-rich florencite-(La) inclusions, within the euclase crystal, expressed as atoms per formula unit (*a.p.f.u.*), and normalised to 14 oxygen atoms. Values were calculated based on EPMA data (n = 9).

Element	Site	Mean a.p.f.u.	±σ	Min	Max
Si	T	0.02	0.01	0.01	0.03
S	T	0.02	0.01	0.01	0.03
P	T	1.19	0.15	1.05	1.37
As	T	0.74	0.14	0.56	0.92
∑T	**T**	**1.97**			
Al	**G**	**2.99**	0.03	2.93	3.22
La	D	0.94	0.03	0.91	1.01
Ce	D	0.01	0	0.01	0.01
Pr	D	0.04	0.01	0.03	0.05
Nd	D	0.08	0.01	0.06	0.09
Ca	D	0.03	0.01	0.02	0.04
Sr	D	0.01	0	0	0.02
∑D	**—**	**1.10**			
O (X)	—	14			
H (X′)	—	5.91			

https://doi.org/10.1180/mgm.2025.10180 Published online by Cambridge University Press

Table 1 presents the full dataset of spot analyses. Normalization to 14 O atoms yielded the average empirical formula is:

$$\mathbf{(La_{0.94}Nd_{0.08}Pr_{0.04}Ca_{0.02}Ce_{0.01}Sr_{0.01})_{\sum 1.10}Al_{2.99}\ (P_{1.19}As_{0.74}S_{0.02}Si_{0.02})_{\sum 1.97}O_{14}H_{5.91}}$$

The H_2O content was calculated by considering six OH groups, with the possibility of additional H atoms introduced by the coupled substitution mechanism $REE^{3+} = M^{2+} + H^{+}$. This process implies that some hydrogen may be structurally incorporated at apical positions of the tetrahedron. Thus, the G, D, and T sites correspond to 3, 1, and 2 cations respectively, distributed over eleven O atoms (eight from the tetrahedra and three from hydroxyl groups), summing to a total of fourteen O atoms in the structural formula. When normalized to an anhydrous basis, charge-balance calculations from the EPMA data indicate only OH groups in the structure, with no requirement for molecular water.

Crystallographic Data

Single-crystal X-ray diffraction analyses yielded the following unit-cell parameters (space group $R\bar{3}m$, Z = 3):

- **Sample 1 (euclase inclusion):** a = 6.9767 Å, c = 16.3495 Å
- **Sample 2 (quartz inclusion):** a = 6.9813 Å, c = 16.3656 Å

The best-fit structural formulae are:

- **Sample 1:** $(La_1)(Al_3)(P_{1.47}As_{0.49})_{\Sigma 1.96}\ O_{14}\ H_{6.2}$
- **Sample 2:** $(La_1)(Al_3)(P_{1.37}As_{0.59})_{\Sigma 1.96}\ O_{14}\ H_{6.2}$

Sample 2 exhibits a slightly lower phosphorous content and correspondingly higher arsenic content, resulting in marginally expanded unit-cell parameters compared to Sample 1. This trend reflects the larger ionic radius of As^{5+} compared to P^{5+}, indicating that

https://doi.org/10.1180/mgm.2025.10180 Published online by Cambridge University Press

compositional variation at the tetrahedral site can influence unit cell dimensions. Crystallographic parameters are listed in Table 3 and the polyhedral bond distances in Table 4.

The D (lanthanide) site was modelled as predominantly occupied by La^{3+}, yielding a distorted dodecahedron with an average La–O distance of 6.6803 Å. Although EPMA data (Table 2) indicate minor amounts of other REE (e.g. Nd, Pr and Ce), attempts to refine mixed La/REE occupancies produced unstable or non-physical parameters, therefore, the final structural model retains La only at the D site.

The TO_4 tetrahedra show variable P and As proportions. The average ⟨As–O⟩ bond lengths are 1.5739 Å in Sample 1 and 1.5783 Å in Sample 2. These values are slightly longer than reported by Scharm et al (1985) for florencite-(La) and shorter than that reported by Mills et al. (2010) for pure arsenoflorencite-(La) (1.668 Å). This supports the interpretation that increasing phosphorous content reduces both ⟨T–O⟩ bond lengths and unit-cell volume. Attempts to refine occupancy by S and Si at the tetrahedral site resulted in significant discrepancies with EPMA data and were not retained in the final model.

The G site forms a distorted octahedron, with Al–O bond lengths averaging 1.893 Å in both samples (Table 4). Bond valence values for mixed P/As site are presented in Table 5 as individual contributions followed by the weighted average. Notably, this indicates that the AlO_6 geometry remains unaffected by the composition of the tetrahedral site. Hydrogen positions were fixed during refinement, as free refinement consistently yielded unrealistic geometries.

https://doi.org/10.1180/mgm.2025.10180 Published online by Cambridge University Press

Table 3. Crystallographic parameters of As-rich florencite (La) in euclase (sample 1) and quartz (sample 2).

Sample	1	2
Formula	$LaAl_3P_{1.47}As_{0.49}O_{14}H_{6.2}$	$LaAl_3P_{1.37}As_{0.59}O_{14}H_{6.2}$
Formula weight (g mol^{-1})	532.28	536.38
Crystal System	Trigonal	Trigonal
Space Group	$R\bar{3}m$	$R\bar{3}m$
a (Å)	6.97670(10)	6.9813(2)
b (Å)	6.97670(10)	6.9813(2)
c (Å)	16.3495(4)	16.3656(6)
α (°)	90	90
β (°)	90	90
γ (°)	120	120
V $(Å)^3$	689.18(3)	690.77(5)
Z	3	3
D_{calc} (g cm^{-3})	3.847	3.868
Crystal Size	0.276x0.214x0.126	0.361x 0.293x 0.201
μ(Mo Kα) / cm^{-1}	7.053	7.353
T_{max}/T_{min}	0.7461/0.6708	0.7454/ 0.5415
Measured reflections/Unique	23205/286	7713 /197
Observed reflections $[F_o^2>2\sigma(F_o^2)]$	286	197
Parameters number	28	28
R $[F_o>2\sigma(F_o)]$	0.0110	0.0128
wR $[F_o^2>2\sigma(F_o)^2]$	0.0330	0.0313
S	1.288	1.244
R_{int}	0.0236	0.0542
RMS (e $Å^{-3}$)	0.090	0.092

https://doi.org/10.1180/mgm.2025.10180 Published online by Cambridge University Press

Table 4. Polyhedral bond distances (Å) in As-rich florencite from samples 1 (in euclase) and 2 (in quartz).

Sample 1			
Dodecahedron (La1)	La1 - O3	2.6590(14)	x 6
	La1 - O2	2.7016(16)	x 6
Octahedron (Al1)	Al1 - O3	1.8876(6)	x 4
	Al1 - O2	1.9038(14)	x 2
Tetrahedron (P/As2)	P/As2 - O1	1.534(3)	x 1
	P/As2 - O2	1.5872(16)	x 3
Sample 2			
Dodecahedron (La1)	La1 - O3	2.6631(18)	x 6
	La1 - O2	2.703(2)	x 6
Octahedron (Al1)	Al1 - O3	1.8883(7)	x 4
	Al1 - O2	1.9037(18)	x 2
Tetrahedron (P/As2)	P/As2 - O1	1.540(4)	x 1
	P/As2 - O2	1.591(2)	x 3

Table 5. Bond valence analysis (v.u.) for As-rich florencite-(La) in sample 1 (euclase) and 2 (quartz).

Sample 1					
	La	Al	P/As	H	$\sum_c v$
O1			1.88/1.21 (avg. 1.37)	0.22	1.59
O2	0.24 x 6	0.50 x 2	1.63/1.05 (avg. 1.19 x 3)		1.93
O3	0.26 x 6	0.53 x 4		0.78	2.10
$\sum_c v$	3.00	3.12	4.94	1.00	
Sample 2					
	La	Al	As/P	H	$\sum_c v$
O1			1.85/1.19 (avg. 1.38)	0.22	1.60
O2	0.24 x 6	0.50 x 2	1.61/1.04 (avg. 1.21 x 3)		1.95
O3	0.26 x 6	0.53 x 4		0.78	2.11
$\sum_c v$	3.00	3.12	5.01	1.00	

Raman Spectroscopy

Raman spectra of As-rich florencite-(La) crystals (Figure 4) were recorded over the 0–3800 cm^{-1} range. A broad feature between 2860 and 3320 cm^{-1} indicates variable hydrogen bonding, mainly due to structural hydroxyls with possible minor contributions from weakly bound or disordered H_2O. By contrast, the sharp band at 3576 cm^{-1} is assigned to a well-defined OH stretching vibration commonly observed for structural hydroxyl in florencite-group minerals. Weak features observed near 1880 and 2334 cm^{-1} fall outside the expected

https://doi.org/10.1180/mgm.2025.10180 Published online by Cambridge University Press

region for the fundamental H–O–H bending mode (≈1600–1650 cm⁻¹) and should therefore be regarded as tentative; they may represent combination/overtone bands or coupling with lattice modes rather than a straightforward δ(H–O–H) assignment. These interpretations are broadly consistent with prior Raman studies of florencite-group and related hydrated phosphates (Frost et al., 2013a,b; Zhukova et al., 2021)

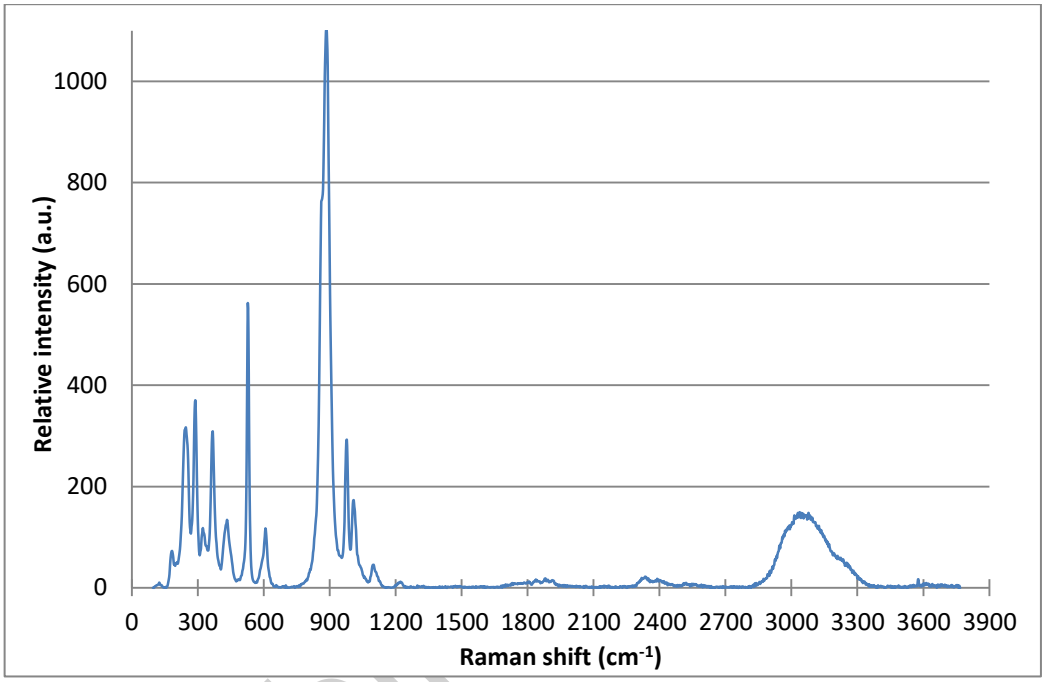

Figure 4. Representative wide-range micro-Raman spectrum of As-rich florencite-(La).

The main Raman bands occur at 888, 859, 537, 289, 246, 368, and 975 cm⁻¹, with secondary features at 180, 326, 430, 608, 824, 944, 1009, and 1098 cm⁻¹. Compared to florencite-(La) spectra reported by Frost et al. (2013a) and Ghignone et al. (2023), the phosphate symmetric stretching band typically observed near 985–987 cm⁻¹ appears at 975 cm⁻¹ in this study. Arsenate-related bands were observed near 870–888 cm⁻¹, while phosphate vibrations are evident between 975 and 1098 cm⁻¹.

Notably, bands at 859 cm⁻¹ and 888 cm⁻¹, attributed to arsenate ions, were not reported in previous florencite-(La) studies. Their presence in both analysed samples confirms arsenate incorporation in the crystal structure. Additional bands in this region may

https://doi.org/10.1180/mgm.2025.10180 Published online by Cambridge University Press

arise from $(PO_3OH)^{2-}$ and $(As_3OH)^{2-}$ groups in disordered tetrahedral sites, as proposed by Frost et al. (2011, 2013b) and Biagioni et al. (2022). However, due to overlap with phosphate and arsenate bands, these features could not be individually resolved and would require infrared spectroscopy for further investigation.

Figure 5 shows detailed Raman spectra in the 0–1250 cm^{-1} range. Minor shifts (up to 9 cm^{-1}) between the two samples were observed, likely due to differences in crystal orientation. Although both samples showed similar band positions, intensity variations, particularly at 528, 888, and 975 cm^{-1}, were noted. These cannot be conclusively attributed to compositional differences due to the non-oriented nature of the analysis.

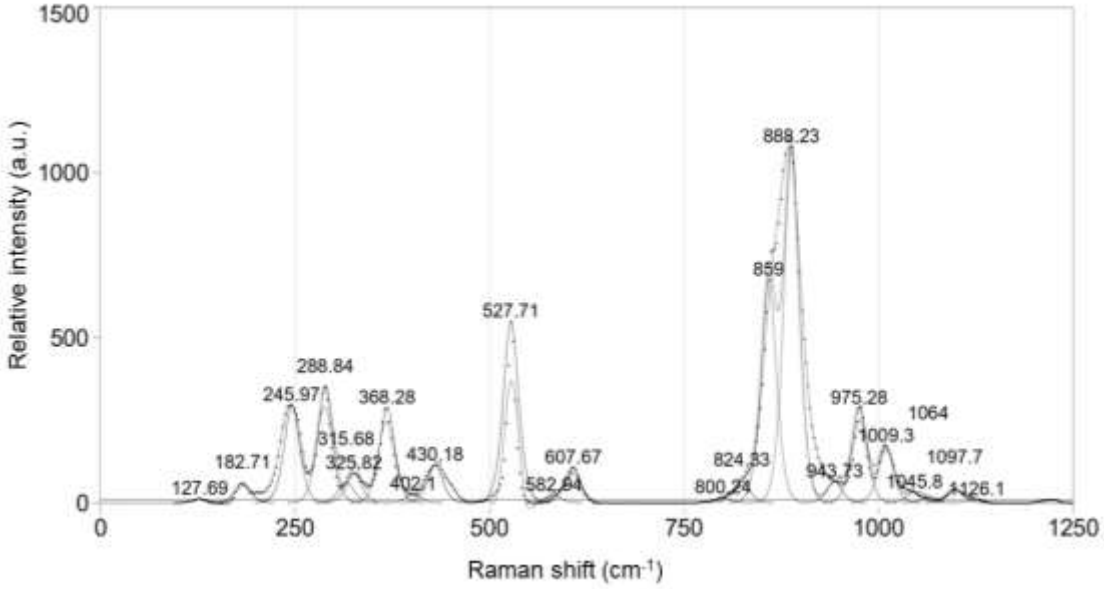

Figure 5. Raman spectrum of As-rich florencite-(La) in the 0-1250 cm-1 range, showing peak positions and relative intesities.

Discussion and conclusions

Electron microprobe analyses and single-crystal X-ray diffraction confirm the occurrence of As-rich florencite-(La) as microscopic inclusions within euclase and quartz crystals from hydrothermal veins hosted in quartzitic layers of the Ouricuri do Ouro Formation, Abaíra County, Bahia, Brazil. Raman spectroscopy further supports this

https://doi.org/10.1180/mgm.2025.10180 Published online by Cambridge University Press

identification by revealing phosphate and arsenate vibrational bands consistent with a solid solution between florencite-(La) and arsenoflorencite-(La). Variations in As and P contents correlate with ⟨T–O⟩ bond lengths and unit-cell expansion, highlighting the structural sensitivity of the alunite supergroup to tetrahedral-site substitutions and the value of crystallographic data in tracing subtle chemical variations in REE-bearing minerals.

The role of hydrogen species in the structure is particularly noteworthy. Charge-balance calculations indicate only structural hydroxyls, yet Raman spectra display weak H_2O-related features, suggesting partial hydration undetectable by EPMA. The absence of a clear Raman band near 1600 cm^{-1} and the broad OH-stretching envelope imply that molecular H_2O is weakly bound or structurally disordered, reflecting variable hydrogen-bonding environments during crystal growth. This apparent discrepancy agrees with the long-recognised ambiguity in hydrogen bonding within the alunite supergroup, where partial proton occupancy and secondary hydrogen-bonding schemes, discussed by Blount (1974) and Mills et al. (2011), have been invoked to satisfy bond-valence requirements.

The marked REE fractionation recorded in these inclusions likely resulted from late-stage hydrothermal fluids under oxidising conditions. Partial oxidation of Ce^{3+} to Ce^{4+} would have stabilised immobile phosphate and fluoride complexes, favouring La-rich phase formation. Similar redox-controlled fractionation was reported for parisite-(La) by Menezes Filho et al. (2018) in the Novo Horizonte region, ~80 km to the north-northwest, suggesting a regional hydrothermal control. Acidic, moderately saline fluids probably enhanced light-REE solubility, leading to La enrichment and precipitation of florencite-(La) at moderate temperatures (200–400 °C) and low pressures. Raman evidence for minor water supports a fluid-assisted crystallisation mechanism for this solid solution.

Collectively, the chemical, structural, and spectroscopic data demonstrate that As-rich florencite-(La) is a sensitive tracer of oxidised, REE-enriched hydrothermal systems. Its

https://doi.org/10.1180/mgm.2025.10180 Published online by Cambridge University Press

occurrence as minute inclusions in euclase and quartz records crystallisation from La-dominant fluids under moderate temperatures and oxidising conditions. These findings extend the known stability field of the florencite group beyond supergene environments and underline its potential as a proxy for redox evolution, fluid–rock interaction, and rare-earth fractionation in hydrothermal systems.

Acknowledgments

The authors express their gratitude to MSc. Susan Martins Drago (Instituto de Geociências, Universidade Federal do Rio Grande do Sul – UFRGS) for conducting the electron probe microanalyses and for her valuable insights. We also thank CETEM, particularly the LMCT and LAPEGE laboratories, for their analytical support and contributions to the discussion of the results. Financial support from the Brazilian Ministry of Science, Technology and Innovation (MCTI) and the National Council for Scientific and Technological Development (CNPq) is gratefully acknowledged.

References

Almeida F.F.M. (1967) Origem e evolução da plataforma brasileira. Rio de Janeiro: DNPM-DGM. Boletim 241.

Almeida F.F.M. (1977) O Cráton do São Francisco. *Revista Brasileira de Geociências*, São Paulo, 7(4): 349-364.

Back M. (2018) *Fleischer's Glossary of Mineral Species*. Tucson, Mineralogical Record, 434 pp.

Bayliss P., Kolitsch U., Nickel E. H. and Pring A. (2010) Alunite supergroup: recommended nomenclature, *Mineralogical Magazine,* **74**, 919– 927.

Biagioni C., Ciriotti M. E., Favreau G., Mauro D., Zaccarini F. (2022) Graulichite-(La), $LaFe_3^{+3}(AsO_4)_2(OH)_6$, a new addition to the alunite supergroup from the Patte d'Oie mine, Bou Skour mining district, Morocco, European Journal of Mineralogy., **34**, 365-374.

Blount, A.M. (1974): The crystal structure of crandallite. Am.Mineral., **59**, 41–47.

Chaves M.L.S.C., Buhn B., Dias C.H. and Menezes Filho L.A. (2018) Idades U-Pb em xenotímio-(Y) de um veio de quartzo com almeidaíta e parisita-(La), novos minerais encontrados na Serra do Espinhaço (Novo Horizonte, BA). *Geociência*s, **37**, 225–236.

https://doi.org/10.1180/mgm.2025.10180 Published online by Cambridge University Press

Chaves, M.L.S.C; Cornejo, C.; Queiroz, L.A.V. (2025) Euclase occurrences in Brazil. Mineralogical Record, 56(3), 247- 280

Dill H.G. (2001) The geology of aluminium phosphates and sulphates of the alunite group minerals: a review. *Earth-Science Reviews*, **53**, 35–93.

Frost R.L., Bahfenne C., Cejka J., Sejkora J., Plasil J., Palmer S., Keeffe E. and Nemec I. (2011) Dussertite $BaFe^{3+}_3(AsO_4)_2(OH)_5$ - a Raman spectroscopic study of a hydroxy-arsenate mineral. *Journal of Raman Spectroscopy*, **42**, 56–61.

Frost R.L., Xi,Y., Scholz R. and Tazava T. (2013a) Spectroscopic characterization of the phosphate mineral florencite-La – $LaAl_3(PO_4)_2(OH, H_2O)_6$, a potential tool in the REE mineral prospection. *Journal of Molecular Structure*, **1037**, 148–153.

Frost R.L., Palmer J.S., Xi Y., Cejka J., Sejkora J. and Plasil J. (2013b) Raman spectroscopic study of the hydroxy-phosphate mineral plumbogummite $PbAl_3(PO_4)_2(OH,H_2O)_6$. *Spectrochimica Acta Part A: Molecular and Biomolecular Spectroscopy*, **103**, 431–434.

Ghignone S., Prencipe M., Manzotti P., Bruno M., Boero F., Borghini A., Costa E., Ciriotti M. and Scaramuzzo E. (2023): The Raman spectrum of florencite-(REE) [REEAl3(PO4)2(OH)6]: An integrated experimental and computational approach. Journal of Raman Spectroscopy, **55**,1-12.

Gilles-Guéry L., Queiroz L.A.V.Q., Schnellrath J., Williams B., Williams C., Barbosa T.C., Laurs B.M., Galoise L. and Calas G. (2022) Pink Orange euclase from Bahia, Brazil. *Journal of Gemmology*, **38**, 44–62.

Guimarães J.T., Alkmim F.F. and Cruz S.C.P. (2012) Supergrupos Espinhaço e São Francisco. Pp. 33–86 in: *Geologia da Bahia, Pesquisa e Atualização* (J.S.F. Barbosa editor). CBPM (Companhia Baiana de Pesquisa Mineral). Salvador, Brazil, 643 pp.

Guimarães J.T., Martins A.A.M., Filho E.L.A., Loureiro H.S.C., Arcanjo J.B.A., Neves J.P.A., Abram M.B., Silva M.G. Melo R.C. and Bento R.V. (2005) *Projeto Ibitiara - Rio de Contas, Estado da Bahia*. CPRM (Serviço Geológico do Brasil) and CPBM (Companhia Baiana de Pesquisa Mineral). Salvador, Brazil, 157 pp. (+ appendixes and maps).

Hussak, E., & Prior, G. T. (1900). Florencite, a new hydrated Phosphate of Aluminium and the Cerium Earths, from Brazil. *Mineralogical Magazine and Journal of the Mineralogical Society*, **12(57)**, 244–248. doi:10.1180/minmag.1900.012.57.04

Jambor J.L. (1999) Nomenclature of the alunite supergroup. *Canadian Mineralogist*, **37**, 1323–1341.

Janeczek J. and Ewing R.C. (1996) Florencite-(La) with fissiogenic REEs from a natural fission reactor at Bangombe, Gabon. *American Mineralogist*, **81**, 1263–1269.

Lefebvre, J.J., Gasparrini, C. (1980) Florencite, an occurrence in the Zairian copperbelt. *The Canadian Mineralogist*, **181**, 301-311.

Menezes Filho L.A.D., Chaves, M.L.S.C., Chukanov, N.V., Atencio, D., Scholz, R., Pekov, I.V., da Costa, G.M. Morrison, S.M., Andrade, M.B., Freitas, E.T.F., Downs, R.T., Belakovskiy, D.I. (2018) Parisite-(La), $CaLa_2(CO_3)_3F_2$, a new mineral from Novo Horizonte, Bahia, Brazil. *Mineralogical Magazine*, **82**, 133-144.

Mills S.J., Kartashov P.M., Kampf A.R. and Raudsepp M. (2010) Arsenoflorencite-(La), a new mineral from the Komi Republic, Russian Federation: description and crystal structure. *European Journal of Mineralogy*, **22**, 613–621.

Nickel E.H. and Temperly J.E. (1987) Arsenoflorencite-(Ce): a new arsenate mineral from Australia. *Mineralogical Magazine*, **51**, 605–09.

Scharm, B.; Kuehn, P.; Scharmova, M.; Novak, L. (1985) Florencite-(La) in the uranium deposits in the Cretaceous of northern Bohemia. Casopis pro Mineralogii a Geologii, 30(2), 163-172.

Smith, D.K., Roberts, A.C., Bayliss, P. and Liebau, F. (1998) A systematic approach to generaland structure-type formulas for minerals and other inorganic phases. *American Mineralogist*, **83**, 126-132.

Süssenberger A., Neves B.B. and Wemmer K. (2014) Dating low-grade metamorphism and deformation of the Espinhaço Supergroup in the Chapada Diamantina (Bahia, NE Brazil): a K/Ar fine-fraction study. *Brazilian Journal of Geology*, **44**, 207–220.

Teixeira J.B.G., Misi A., Silva M.G. and Brito R.S.C. (2019). Reconstruction of Precambrian terranes of Northeastern Brazil along Cambrian strike-slip faults: a new model of geodynamic evolution and gold metallogeny in the State of Bahia. *Brazilian Journal of Geology*, **49**, 1–21. https://doi.org/10.1590/2317-4889201920190009.

Torquato J.R. and Fogaça A.C.C. (1981) Correlações entre o Supergrupo Espinhaço no Brasil, o Grupo Chela em Angola e as formações Nosib e Khoabendus da Namíbia. Pp. 87-98 in: Simpósio sobre o Craton do São Francisco e suas faixas marginais. Salvador, Brasil,.

Trompette R. (1994) Geology of western Gondwana (2000-500 M.a): Pan-African-Brasiliano aggregation of South America and Africa. Balkema: Rotterdam.

Zhukova, I. A., Stepanov, A. S., Korsakov, A. V., & Jiang, S. Y. (2022). Application of Raman spectroscopy for the identification of phosphate minerals from REE supergene deposit. Journal of raman Spectroscopy, 53(3), 485-496.

https://doi.org/10.1180/mgm.2025.10180 Published online by Cambridge University Press